

# Direct and pulse plating of metastable Zn–Ni alloys

S. Ieffa, R. Bernasconi, L. Nobili, P. L. Cavallotti and L. Magagnin\*

## Introduction

A widely used method to protect steel surfaces from corrosion is the application of a sacrificial layer of a less noble metal, which undergoes preferential corrosion due to galvanic coupling. The most used material is zinc, a metal readily available and easy to apply on components presenting large areas. However, zinc is far more reactive than iron, and the thickness of material needed to effectively prevent corrosion represents an issue for some applications, such as coatings for the automotive sector or the aerospace field. A possible solution can be the alloying of zinc with a metal of the iron group, thus increasing the nobility of the layer. By doing this the corrosion potential is shifted to values closer to iron, inducing a slower consumption of the sacrificial layer. Nickel, having a suitable equilibrium potential, is the most used metal,<sup>1–4</sup> providing an excellent corrosion protection with respect to pure zinc. The coatings obtained are 5–6 times more resistant to corrosion than pure zinc and are currently studied as alternatives to cadmium.<sup>5</sup> Zn–Ni alloys are reasonably easy to electrodeposit, and the plating of corrosion efficient coatings was performed in the past from acidic<sup>6,7</sup> and alkaline<sup>8,9</sup> electrolytes. It is well-known that the best protective properties are achieved when the alloy presents a single  $\gamma$  phase, a condition that can be attained by controlling properly the plating parameters and electrolyte formulation.<sup>10,11</sup> It is interesting to point out that the plated  $\gamma$

phase can be a metastable structure, as the Zn–Ni phase diagram predicts lattice distributions of the Ni atoms in contrast with the experimental results.<sup>12,13</sup> The reasons for the observed metastability and the thermodynamic properties of Zn–Ni have been elucidated previously<sup>9</sup> starting from the analysis of the equilibrium conditions of the different phases. It was demonstrated that Zn–Ni electroplated alloys from an alkaline bath follow the theoretical simulations, thus validating the interpretation provided.

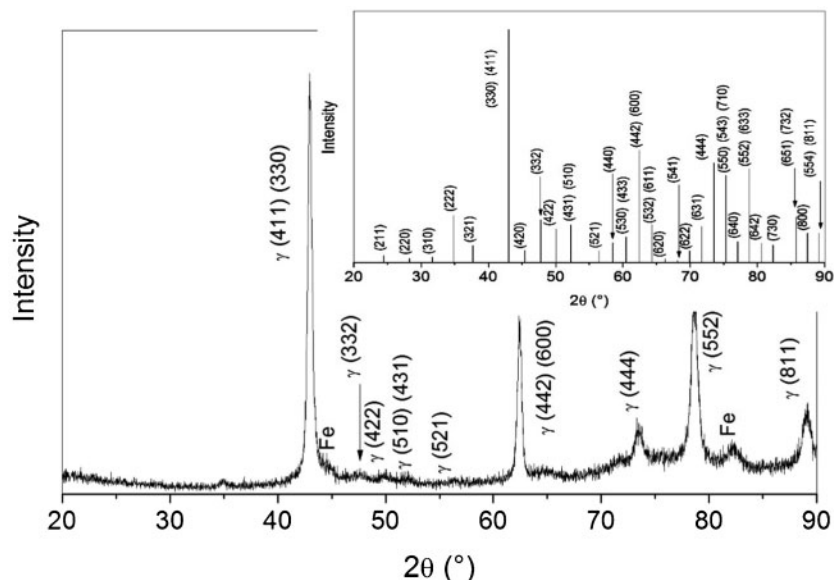
Zn–Ni can be plated also by means of pulsed electrodeposition,<sup>14–16</sup> a method suitable to achieve more refined microstructures and compact layers. This change in microstructure also improves the corrosion behaviour<sup>17</sup> and the distribution of the residual stresses.<sup>18</sup> The aim of the present research is the investigation of the differences in microstructure and corrosion properties when using pulse plating instead of direct electrodeposition in an alkaline solution.<sup>9</sup> The thermodynamics of the alloys obtained, with particular emphasis on deviations from the DC plating case, are also part of the analysis. Finally, a corrosion study suitable to underline any corrosion improvement coming from the use of PC plating is provided.

## Experimental methods

DC plated coatings for microstructure analysis and theoretical discussion were deposited from a cyanide-free commercial bath (GLOVEL 800 by Glomax srl). This was an alkaline solution containing zinc oxide, nickel sulphate, sodium hydroxide, complexing agent (amine) and proprietary additives. The operating temperature was 25°C and the deposition rate 0.3  $\mu\text{m min}^{-1}$

Dip. Chimica, Materiali e Ing. Chimica Giulio Natta - Politecnico di Milano, Via Mancinelli 7, 20131 Milano, Italy

\*Corresponding author, email luca.magagnin@polimi.it



1 Pattern (XRD) of as-deposited Zn–Ni and calculated XRD spectrum (inside) of  $\gamma$  structure with randomly distributed Ni atoms

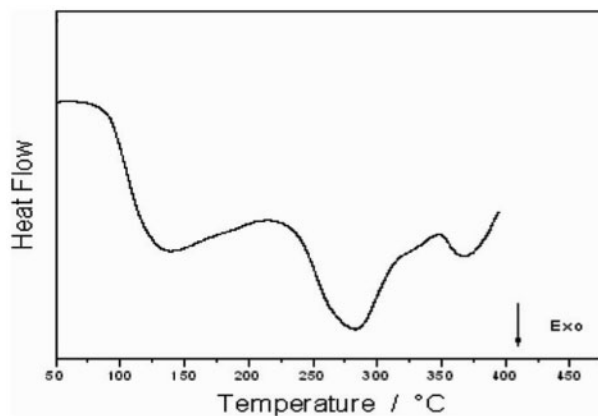
at a current density of  $2 \text{ A dm}^{-2}$  ( $20 \text{ mA cm}^{-2}$ ). Coatings with nickel content between 14 wt.-% (15.4 at.-%) and 17 wt.-% (18.6 at.-%) could be deposited from this bath. Such coatings can achieve outstanding corrosion resistance, enduring more than 1000 h of exposure in neutral salt spray chamber without signs of red rust. Coatings were tested in the as-deposited condition and after substrate removal and subsequent annealing in nitrogen for 1 h at  $400^\circ\text{C}$ . Differential scanning calorimetry (DSC) was used to investigate the thermal stability of the substrate-free Zn–Ni coatings. The heating rate was  $10^\circ\text{C min}^{-1}$ .

Zn–Ni alloys in pulse plating conditions were electro-deposited from an alkaline additive-free electrolyte composed of  $15 \text{ g L}^{-1}$  ZnO,  $1.5 \text{ g L}^{-1}$   $\text{NiSO}_4 \cdot 6\text{H}_2\text{O}$ ,  $130 \text{ g L}^{-1}$  NaOH and  $50 \text{ g L}^{-1}$  triethanolamine TEA. All the chemicals were purchased from Sigma Aldrich and used as-received. The operating temperature was  $25^\circ\text{C}$ , while the current density was  $25 \text{ mA cm}^{-2}$  for DC deposition on carbon steel from such additive-free electrolyte. Different duty cycles were tested for PC deposition. The nickel content was analysed by energy dispersive X-ray spectroscopy (EDS) using an Oxford INCA Energy 200 EDS unit mounted on a Zeiss EVO 50 EP scanning electron microscope. Crystalline structure was analysed by X-ray diffraction (XRD) using  $\text{Cu } K_\alpha$  radiation. The instrument used for the purpose was a diffractometer (Philips PW 1830), equipped with a vertical goniometer PW 1820. Corrosion tests were performed using a Princeton Analytical EG&G potentiostat/galvanostat using Pt as counter electrode and SCE as reference. The solution used was 3.5 wt.-% NaCl and scan rate was  $1 \text{ mV s}^{-1}$ , because of anticipated good corrosion resistance of the alloys and no expected significant effects on the electrochemical comparison between the two alloys.

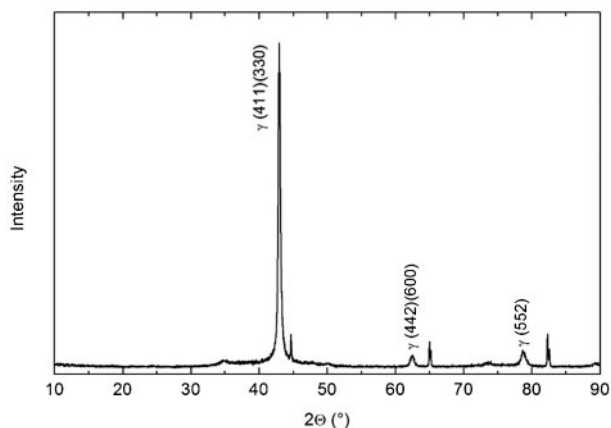
## Results and discussion

The compositions examined in this work are characterised by a nickel percentage very close to the composition of the intermetallic  $\text{Ni}_5\text{Zn}_{21}$  (19.2 at.-%).

The Zn-rich part of the phase diagram is composed for temperatures up to  $400^\circ\text{C}$  of the solid solution with hexagonal close packed (hcp) structure and very low solubility of Ni ( $\eta$  phase), the monoclinic  $\delta$  phase (10–11 at.-% Ni) and the cubic  $\gamma$  phase (15–26 at.-% Ni).<sup>19</sup> The plated film is therefore expected to be composed of the cubic  $\gamma$  phase. This is in part true, as seen from the XRD data reported in Fig. 1. The spectrum was obtained from a sample plated from the commercial Zn–Ni solution containing complexing agent (amine) and proprietary additives<sup>9</sup> described above (Glovel 800). In the graph only peaks belonging to  $\text{Ni}_5\text{Zn}_{21}$  (JCPDS 6-0653) can be observed, together with the Fe features of the substrate. It is important to point out that the peak at  $34.95^\circ$  cannot be identified, and some high-intensity reflections of the  $\gamma$   $\text{Ni}_5\text{Zn}_{21}$  phase are not present. The diffraction spectrum becomes identical to the theoretical one only after an annealing at  $400^\circ\text{C}$  in a nitrogen atmosphere, suggesting the possibility of a metastable behaviour for the alloy. This has been verified<sup>9</sup> by means of DSC and thermodynamic calculations based on the experimental data from samples obtained from a cyanide-free commercial bath (Glovel 800). As shown in Fig. 2, DSC in particular showed the presence of



2 Trace (DSC) obtained from Zn–Ni coating

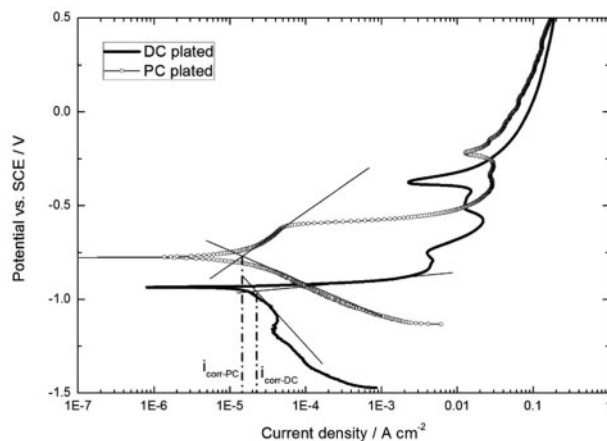


**3 Pattern (XRD) of as-deposited Zn–Ni alloy from additive-free electrolyte in pulse plating conditions:  $t_{\text{on}}=6$  ms at  $15 \text{ mA cm}^{-2}$ ,  $t_{\text{on}}=1$  ms at  $-7.5 \text{ mA cm}^{-2}$ ,  $t_{\text{off}}=2$  ms**

exothermic transformations between a metastable structure and the proper  $\gamma$  phase. Considering the possible contribution of grain growth to the enthalpy change measured by DSC analysis, its effect was estimated from line broadening in the XRD spectra. By using the Scherrer equation, the average crystallite size was found to be 34 nm in the as-deposited alloy, which increased to 61 nm after annealing. An enthalpy change of  $-0.11 \text{ kJ mol}^{-1}$  was evaluated by employing experimental values of grain boundary energy in zinc. This rough calculation shows that grain growth represents a small part of the total enthalpy change ( $-4.2 \text{ kJ mol}^{-1}$ ), thus confirming our hypotheses of an ordering transformation of the electrodeposited phase expected to occur by a nucleation and growth mechanism or a continuous ordering reaction, according to the transformation temperature.

However, the atomic structure of the  $\gamma$  phase is relatively complex and the ordering transformation of the Zn–Ni alloy would imply atomic rearrangement over several sub-lattices. Further investigation is required to elucidate these features and to correlate the transformation steps to the exothermic peaks in the DSC trace. In the stable phase, Ni atoms occupy the outer tetrahedral positions of the bcc structure, minimising the number of Ni–Ni contacts.<sup>20</sup> Metastability suggests a higher enthalpy content in the electroplated alloy, with the Ni atoms able to occupy all the sub-lattice positions with equal probability. These considerations were applied to the simulation of the X-ray structure factors and diffraction intensities. The calculated diffraction pattern is shown in Fig. 1 (Ni atoms randomly distributed over all atomic sites). All peaks of the as-deposited alloy correspond to diffraction lines of the calculated spectrum, including the reflection at  $34.95^\circ$ .

The same approach can be applied to the coatings obtained by pulse plating in additive-free electrolytes. Figure 3 reports the XRD pattern of a Zn–Ni alloy with 16 wt-% nickel obtained using the following cycle:  $t_{\text{on}}=6$  ms at  $15 \text{ mA cm}^{-2}$ ,  $t_{\text{on}}=1$  ms at  $-7.5 \text{ mA cm}^{-2}$ ,  $t_{\text{off}}=2$  ms. From the comparison of XRD spectra in Figs. 1 and 3, it can be observed that pulse plating allows us to obtain a Zn–Ni deposit with a metastable crystalline structure such as the one produced in a commercial electrolyte by DC plating. Commercial electrolytes



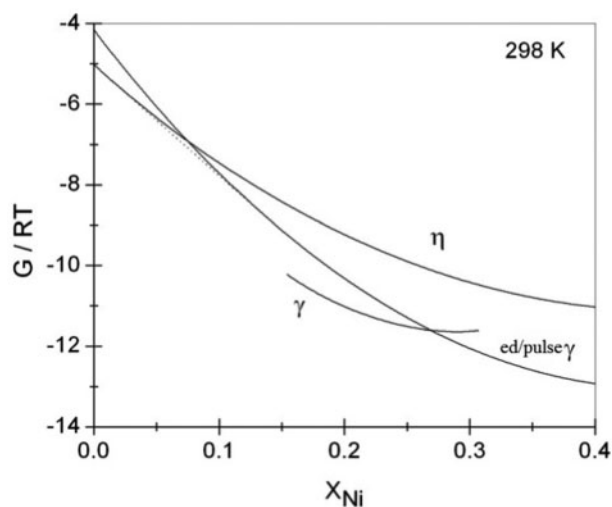
**4 Potentiodynamic curves in NaCl 3.5% solution on as-deposited Zn–Ni alloy from an additive-free electrolyte in DC plating and PC plating conditions:  $t_{\text{on}}=6$  ms at  $15 \text{ mA cm}^{-2}$ ,  $t_{\text{on}}=1$  ms at  $-7.5 \text{ mA cm}^{-2}$ ,  $t_{\text{off}}=2$  ms**

working in DC conditions can tailor the properties of the electrodeposits and the crystalline structure by a combination of complexing agents and additives; the same effects on atomic arrangement and Ni–Ni pairs deposition can be achieved by pulse plating, optimising direct and reverse pulses, introducing also a preferential crystalline orientation along the (411)/(330) planes.

The metastable  $\gamma$  phase obtained by pulse plating in additive-free electrolytes can affect the corrosion behaviour of the coating, usually increasing the corrosion resistance in agreement with results obtained with DC plating in commercial solution, as shown in Fig. 4.

Figure 4 also shows that DC plating in additive-free electrolytes does not produce the  $\gamma$  phase with the same properties of the metastable one achieved by pulse plating.

Free energy curves calculated at 298 K are reported in Fig. 5. This plot shows that the metastable equilibrium between the hcp solid solution ( $\eta$ ) and the DC



**5 Molar Gibbs free energy at 298 K as function of nickel atomic fraction for different phases: hcp solid solution ( $\eta$ ), equilibrium  $\gamma$  phase ( $\gamma$ ) and DC/PC electrodeposited  $\gamma$  phase (ed/pulse  $\gamma$ ). Common tangent between  $\eta$  and ed/pulse  $\gamma$  is shown as dotted line**

electrodeposited/pulse plated  $\gamma$  phase (ed/pulse  $\gamma$ ) entails the existence of  $\eta$  from 0 to 1.5 at.-%Ni,  $\eta$ +ed/pulse  $\gamma$  from 1.5 to 13.5 at.-%Ni and ed/pulse  $\gamma$  at higher Ni content. This prediction is in agreement with experimental results about the electrodeposition of Zn–Ni alloys with different composition.

## Conclusions

Zn–Ni alloys with single  $\gamma$  phase were deposited from an alkaline electrolytic bath in DC and PC conditions. X-ray diffraction and DSC results show that the electrodeposited phase exhibits different atomic distribution and enthalpy content compared with the equilibrium  $\gamma$  compound, due to a random distribution of Ni atoms over the sub-lattice positions of the  $\gamma$  structure. This behaviour can be obtained in commercial electrolytes containing complexing agents and additives by DC plating, and in additives-free electrolytes by the use of optimised pulse plating conditions. The pulse plated metastable  $\gamma$  phase shows the same corrosion resistance improvement as the one obtained by DC plating in commercial solutions. The Gibbs free energy of the electrodeposited phase was evaluated and the metastable phase boundaries were obtained for DC and PC plated deposits. Reasonable agreement was found with experimental values reported in the literature.

## Acknowledgement

This paper is based on a presentation given at the 6th European Pulse Plating Seminar, Baden, Austria, 7th March 2014.

## References

1. A. Conde, M. A. Arenas and J. J. de Damborenea: *Corros. Sci.*, 2011, **53**, 1489–1497.
2. M. Gavrilu, J. P. Millet and H. Mazille: *Surf. Coat. Technol.*, 2000, **123**, 164–172.
3. R. M. Gnanamuthu, S. Mohan and G. Saravanan: *J. Alloys Compd.*, 2012, **513**, 449–454.
4. O. Hammami, L. Dhouibi and E. Triki: *Surf. Coat. Technol.*, 2009, **203**, 2863–2870.
5. G. F. Hsu: *Plat. Surf. Finish.*, 1984, **71**, 52–55.
6. S. Ghaziof and W. Gao: *Appl. Surf. Sci.*, 2014, **311**, 635–642.
7. A. Chitharanjan Hegde, K. Venkatakrishna and N. Eliaz: *Surf. Coat. Technol.*, 2010, **205**, 2031–2041.
8. K. R. Sriraman, H. W. Strauss, S. Brahim, R. R. Chromik, J. A. Szpunar, J. H. Osborne and S. Yue: *Tribol. Int.*, 2012, **56**, 107–120.
9. L. Magagnin, L. Nobili and P. L. Cavallotti: *J. Alloys Compd.*, 2014, **615**, S444–S447.
10. X. Qiao, H. Li, W. Zhao and D. Li: *Electrochim. Acta*, 2013, **89**, 771–777.
11. L. M. Chang, D. Chen, J. H. Liu and R. J. Zhang: *J. Alloys Compd.*, 2009, **479**, 489–493.
12. C. Bories, J. P. Bonino and A. Rousset: *J. Appl. Electrochem.*, 1999, **29**, 1045–1051.
13. P. L. Cavallotti, L. Nobili and A. Vicenzo: *Electrochim. Acta*, 2005, **50**, 4557–4565.
14. Y. F. Jiang, L. F. Liu, C. Q. Zhai, Y. P. Zhu and W. J. Ding: *Thin Solid Films*, 2005, **484**, 232–237.
15. H. Ashassi-Sorkhabia, A. Hagraha, N. Parvini-Ahmadib and J. Manzoori: *Surf. Coat. Technol.*, 2001, **140**, 278–283.
16. S. O. Pagotto Jr, C. M. de Alvarenga Freire and M. Ballester: *Surf. Coat. Technol.*, 1999, **122**, 10–13.
17. J. B. Bajat, A. B. Petrovic and M. D. Maksimovic: *J. Serbian Chem. Soc.*, 2005, **70**, 1427–1439.
18. S. E. Hadian and D. R. Gabe: *Surf. Coat. Technol.*, 1999, **122**, 118–135.
19. T. B. Massalski, J. L. Murray, L. H. Bennett and H. Baker: 'Binary alloy phase diagrams'; 1986, Metals Park, OH, American Society for Metals.
20. A. Johansson, H. Ljung and S. Westman: *Acta Chem. Scand.*, 1968, **22**, 2743–2753.